FOREBODY VORTEX MANAGEMENT FOR YAW CONTROL AT HIGH ANGLES OF ATTACK

ICAS-86-2.5.2

Dhanvada M. Rao
Vigyan Research Associates, Inc., Hampton, Virginia 23666-1325

Cary Moskovitz
North Carolina State University, Raleigh, North Carolina 27650

Daniel G. Murri
NASA Langley Research Center, Hampton, Virginia 23665-5225

Abstract

The yaw-control potential of deployable forebody strakes at angles of attack above the range of conventional rudder effectiveness has been investigated. The conformally-stored strakes when deployed force asymmetrical vortex shedding from the forebody, thereby generating a controlled yawing moment. The concept was explored through low-speed wind tunnel tests on a conical forebody in isolation and in a generic fighter configuration. Force and moment measurements on the complete model were supplemented with circumferential pressure and flow-visualization surveys on an isolated forebody, in order to gain insight into the vortex flow mechanisms resulting from forced asymmetrical separations and to quantify the obtainable yaw power at angles of attack to 80^{o}. This preliminary, low-Reynolds-number study showed asymmetrically-deployed forebody strakes to have considerable yaw control potential, whose sensitivity to scale effects needs further investigation.

Nomenclature

C_{ℓ}	Rolling moment coefficient
C_m	Pitching moment coefficient
C_n	Yawing moment coefficient (body axis)
C_p	Pressure coefficient
α	Angle of attack, deg.
β	Angle of sideslip, deg.
δ_s	Strake deflection angle, deg.
ϕ	Forebody circumferential angle from windward meridian, deg.
ϕ_s	Strake circumferential position, deg.

I. Introduction

Considerable interest currently exists in the developement of aerodynamic techniques for enhanced controllability of next-generation combat aircraft, particularly in the context of post-stall maneuverability requirements. An example of control deficiency limiting the present-day maneuverability of fighters is the loss of rudder effectiveness due to increasing submergence of the vertical tails into the low-energy wing wake at high angles of attack. Often, this phenomenon occurs when a typical highly-swept configuration also is tending towards directional instability. Consideration must therefore be given to evolving alternate aerodynamic means of providing yaw control and stability augmentation systems which eliminate directional instability.

This paper addresses the possibility of manipulating the characteristic steady-state vortex system of slender forebodies at high angles of attack, in order to generate controlled side forces well forward of the aircraft center of gravity and thereby provide an alternative source of yawing moment. The aerodynamic potential of naturally-occuring high-alpha vortex asymmetry on slender bodies is well known (e.g. Ref. 1); the technical challenge is to harness this potential in a practical manner and convert it into a precisely controllable source of yaw power. This concept was demonstrated in Ref. 2, by the use of jet blowing on a specific forebody shape of relatively high fineness ratio and a horizontally-elliptical cross section. Such forebodies are characterized by a powerful vortex asymmetry (Ref. 3), which offers favorable conditions for applying the fluid-amplification principle represented by jet blowing. On other forebody geometries which preclude the development of a naturally strong vortex asymmetry, however, vortex manipulation to generate effective yaw control requires a different approach.

An alternative concept proposed herein involves creating a vigorous vortex system on a given forebody, and manipulating the vortex system in an asymmetrical sense to generate the desired control effectiveness. This may be accomplished by means of deployable forebody strakes, as shown in Fig. 1. Narrow, sharp-edge strakes affixed to forebodies and fuselage aft-ends have frequently been employed to improve the high-angle-of-attack handling and spin characteristics by fixing separation and controlling the vortex shedding. The strakes in the present concept are suitably pivoted and deployable at command from their conformally-stored position on the forebody. The sharp edge of the deployed strake forces cross-flow separation and also amplifies the shed vorticity. The strength and position of the forced vortex may be regulated within limits by varying the strake deflection angle. Two basic modes of strake deployment are indicated in Fig. 1. Asymmetric deployment (i.e., one strake out at a time) will force strong flow asymmetry and thus generate a side force which may be modulated via strake deflection. Simultaneous deployment (i.e., both strakes out) will establish a symmetrical forebody separation pattern with augmented vortices, from which a controlled side force may be extracted via anti-symmetric (or differential) strake deflection.

The circumferential location (ϕ_s) of the forebody strakes would seem to be an important variable governing the side-force development over a range of alpha. The side-force modulation capability through variation of strake deflection

angle (δ_s) is of interest from the viewpoint of precision of control. The relative merits of the two aforementioned strake deployment options, viz., asymmetric and symmetric, also need assessment. The foregoing parameters were initially addressed in an exploratory investigation of the deployable strake concept, using an axi-symmetric conical forebody for simplicity. The initial force and moment results have been reported in Ref. 4; this paper presents results subsequently obtained, which emphasize the forebody flow-field aspects.

The low Reynolds number of the present study is to be noted. Whereas the cross-flow separation and vortex characteristics of smooth and rounded slender bodies are known to be highly Reynolds number dependent (Ref. 1), forced separations viz., with strakes are generally regarded to be relatively less sensitive. In the case of asymmetric strake deployment when free separation still occurs on one side of the forebody, however, Reynolds number effects must be anticipated. Although the current results are believed to provide a valid assessment of the basic concept, they must ultimately be evaluated with respect to scale effects.

II. Experimental Details

The geometry and principal dimensions of the wind-tunnel model employed in this investigation are shown in Fig. 2. The generic fighter configurations were tested on a 6-component strain gage balance in the NASA Langley 12-foot Low Speed Tunnel, using standard instrumentation and data acquisition techniques. Two alternate flat-plate wing planforms, viz., a trapezoidal and a 60° delta, were tested on a common fuselage; the former configuration included the full empennage as shown, whereas the latter had only the vertical tail/rudder. The 9° semi-angle conical forebody had longitudinal surface slots to hold sheet-metal strakes at selected ϕ_s positions. A set of strakes bent to specific positive and negative δ_s angles was provided.

The isolated forebody pressure model (Fig. 3) was tested on a sting in the North Carolina State University subsonic tunnel at 50° angle of attack. In addition to pressure measurements with single and double strakes in a variety of ϕ_s and δ_s settings, this model also was used for flow visualizations. Certain unusual features of cross-flow visualization technique used in the present investigation may be of interest: the 1-inch thick light sheet used to illuminate the cross-flow plane was considerably thicker than normally employed, while the flow was seeded with helium bubbles rather than smoke. Thus, the bubble pathlines were captured in long-exposure photographs with the steady-state vortex cores standing out clearly as concentrated circular streaks against a background of short vertical lines representing the cross-flow component of free-stream velocity. This somewhat unusual but simple adaptation of a standard visualization technique greatly aided the understanding of flow mechanisms underlying the present study.

The test Reynolds numbers in the various phases of this study, based on fuselage diameter, were as follows:

Balance Tests	- 190,000
Forebody Pressures	- 109,000
Flow Visualization	- 41,000

III. Flow Field Characteristics

Some insight into the forced asymmetrical cross-flow separations and related vortex characteristics due to forebody strakes can be gained through the coordinated flow visualization and circumferential pressure surveys obtained at a fixed angle of attack of 50°, selected results of which will be discussed here. For reference, the basic forebody (i.e., no strakes) data are presented in Fig. 4, which shows the vortex asymmetry expected at an angle of attack which greatly exceeds the cone semi-angle.

A comparison of $\phi_s = 60°$ and 90° positions of the single strake deployment is presented in Fig. 5. Although only 30° apart in ϕ_s, these two strake positions generate fundamentally different types of asymmetry, as evident in the corresponding circumferential pressure distributions. With $\phi_s = 60°$, the forced separation increases the suction level on the strake side while reducing it on the opposite (smooth) side of the forebody, which will produce a negative side force. Just the opposite occurs at $\phi_s = 90°$, i.e., the suction is reduced on strake side of the forebody but enhanced on the smooth side, the net effect being a positive side force.

A clue to this contrasting behavior may be found in the distinctive strake vortex flow characteristics generated in the two cases as illustrated in Fig. 6. With $\phi_s = 60°$, the strake vortex occurs close to the forebody and is followed by flow re-attachment at a circumferential position approaching 180°. A significant portion of the left-half of forebody is covered by a shallow separation bubble, which effectively presents a moving boundary in the direction of external cross-flow. This effect is manifested as a clockwise circulation, which will tilt the cross-force vector to the left of the incidence plane, thus, generating a negative sideforce.

In the case of $\phi_s = 90°$, however, the strake vortex is considerably larger and situated off the forebody; the forced separation does not re-attach, and a saddle point appears in the wake. Here, the strake evidently functions as a spoiler and thus creates an effective circulation in the opposite direction (see Ref. 5). The 'strake-vortex' mechanism (A) would be expected to generate significant side force primarily in the alpha range where stable forebody vortices occur, whereas the 'spoiler' mechanism (B) should be effective at angles of attack approaching 90°.

The effect of strake deflection is now considered for the case of $\phi_s = 90°$. As shown in Fig. 7, positive deflection of the strake moves its vortex towards the leeward meridian ($\phi \rightarrow 180°$) where its suction presumably is able to influence and alleviate flow separation on the right-hand side of the forebody. This reinforces the counter-clockwise circulation effect and thus increases the positive sideforce. Conversely, negative strake deflection causes the right-side separation to occur earlier, as evidenced by its

augmented vortex. These systematic induced-suction effects on the opposite half of forebody indicate a side-force modulation capability through strake deflection.

The case of double-strake deployment at $\phi_s = 90^o/270^o$ is presented in Fig. 8. Here, $\delta_s = 0^o$ on either side represents the baseline case, with a symmetrical pair of augmented vortices. Anti-symmetric strake deflection (left strake up, right strake down), causes the left vortex to be raised away while the right vortex is brought closer to the forebody. However, the induced asymmetry of pressure distributions on either half is not as marked as with a single strake at $\phi_s = 90^o$, implying that the side-force potential of double strakes will be less.

Pressure distributions for a single strake at $\phi_s = 120^o$ are shown in Fig. 9. The strake evidently continues to function as a spoiler generating a higher level of suction on the opposite side of the forebody. Positive deflection of the strake (to 60^o) is found to produce almost equal but opposite effects on either side of the forebody, indicating a sensitive sideforce modulating capability.

The double strake case ($\phi_s = 120^o/240^o$) is shown in Fig. 10. An anti-symmetric deflection (left strake up, right strake down) progressively increases the left-side suction; however, the degree of asymmetry (and accordingly the side-force potential) is again not as pronounced as with a single strake.

Flow visualizations in the cross-flow plane as well as in side views for the double strakes ($\phi_s = 120^o/240^o$) at $\alpha = 50^o$ are presented in Fig. 11. The vortex off the up-deflected (left) strake is seen to be drawn towards the forebody and generates the high suction peaks observed in the left-half pressure distribution. In the side view, this vortex is identified as having a tightly-wound core; the vortex from the down-deflected strake is relatively diffused and not as readily visualized.

IV. Force and Moment Measurements

Isolated Fuselage

The purpose of these initial tests was to confirm the trends with respect of ϕ_s and δ_s inferred from the pressure surveys, and also to assess the yawing moment effectiveness of forebody-strake generated asymmetries through an extended angle-of-attack range.

The effect of a single strake with ϕ_s varied from 60 to 90^o is shown in Fig. 12. These data* confirm the reversal of asymmetry when the strake is moved from $\phi_s = 60$ to 90^o. Also shown is an intermediate case of $\phi_s = 80^o$ where the asymmetry changes direction with increasing angle of attack, presumably as a result of the flow changing from mechanism 'A' to mechanism 'B'. In any event, $\phi_s = 80^o$ is clearly an undesirable location for the asymmetric strake.

*Note: Reference area used with isolated fuselage data is same as trapezoidal wing area.

Although the overall yaw power with $\phi_s = 60^o$ and 90^o are roughly comparable, a distinct difference can be noted with respect to the angle of attack effect. The yawing moment capability above $\alpha = 60^o$ is better retained in the case of $\phi_s = 90^o$, which lends credence to the hypothesized 'spoiler' flow mechanism (B). The anticipated weakening of 'strake-vortex' mechanism (A) due to lifting away of the vortex core from the forebody at higher angles of attack is evident in the result for $\phi_s = 60^o$.

The typical effect of strake deflection at $\phi_s = 90^o$ is presented in Fig. 13. Since strake deflection essentially controls the vortex position, its modulating capability would be expected to degrade at the higher angles of attack when the vortex mechanism is less effective, as confirmed in Fig. 13.

The results with an asymmetric strake located at $\phi_s > 90^o$ are presented in Fig. 14. A marked improvement in the high-alpha yawing-moment capability is found with ϕ_s increased to 120^o, as expected from the substantial pressure asymmetry across the forebody observed for this case (Fig. 9). The case of double-strakes at $\phi_s = 120^o/240^o$ is presented in Fig. 15. Included for reference is the basic forebody (i.e. strakes off) yawing moment characteristics, showing the typically cyclic asymmetry encountered through the alpha range. Double strakes deployed symmetrically (i.e. at zero deflection) substantially reduce these asymmetries, indicating a significant strake influence on the vortex wake development. The yaw effectiveness generated in both directions by anti-symmetrical strake deflections is sustained to the highest angle of attack (in spite of a directional bias probably due to asymmetrical wake interaction with the aft fuselage). The magnitude of yawing moment (as measured from the zero-deflection datum) however, is only about 50 percent of that produced by an asymmetrical strake.

Trapezoidal Wing Configuration

Results for the case of $\phi_s = 105^o$ single strake have been selected to illustrate the yaw control capability on the trapezoidal wing configuration. The yawing moment results presented in Fig. 16 compare the forebody-strake and rudder characteristics. The onset of forebody-strake effectiveness coincides with the decline of rudder power above $\alpha = 10^o$, and attains a peak value considerably in excess of the low-alpha rudder power just when the latter is reduced to zero. Even at $\alpha > 50^o$ the strake continues to generate a yaw power comparable with the rudder at zero alpha. Also seen is the yaw modulation capability from $\alpha = 30^o$ to the maximum angle of attack of the test.

Since post-stall maneuvering usually involves considerable side-slip excursions, the effectiveness of yaw control at large positive and negative side-slip angles is important. The effect of side-slip at a constant 50^o angle of attack on the yaw control power of the $\phi_s = 105^o$ asymmetric strake is shown in Fig. 17. The yaw control is found to be maintained up to nearly 20^o of side-slip angle in either direction.

Delta Wing Configuration

The change from trapezoidal to delta wing configuration resulted in two consequences: the effective forebody length was reduced by approximately 50 percent, and the reference wing area increased 88 percent. Forebody length reduction would be expected to degrade the aerodynamic effectiveness of yaw strakes; the yawing moment coefficient will be further reduced by the increase in reference area. Nevertheless, the forebody yaw capability can still be assessed in comparison with rudder effectiveness on the same configuration. The delta-wing yawing moment coefficients shown in Fig. 18, although substantially less in absolute values than those obtained with the trapezoidal configuration for the above-mentioned reasons, remain comparable with the rudder power. A comparison of the single and double strake arrangements again indicates the former to be more effective for yaw control, certainly in the intermediate-alpha (α = 40 to 60^{o}) range.

The induced-roll characteristics are shown in Fig. 19. The rudder produces an adverse rolling moment throughout its useful alpha range, whereas the single strake deployment generates a proverse roll. It may also be recalled that whereas the rudder side-force is in opposition to the direction of turn, the forebody sideforce is pro-turn. Thus, the indirect effects which occur when deploying the forebody strake for yaw control should be favorable to high-alpha handling characteristics. Although the pitching moment characteritics, shown in Fig. 20, indicated a nose-up increment due to strake deployment, its magnitude was quite small.

V. Concluding Remarks

An exploratory low-speed wind tunnel study was conducted to evaluate a deployable forebody strake concept for yaw control at angles of attack above the range of conventional rudder effectiveness. Flow visualizations and circumferential pressure surveys on an isolated conical forebody were combined with force and moment measurements on generic fighter configurations incorporating the same forebody geometry, to acquire insight into the forced asymmetric forebody flow separation and to evaluate its yaw control potential. The variables studied were the circumferential location of the strake on the forebody and strake deflection angle; the data were analyzed for the most advantageous development of sideforce with angle of attack and for sideforce modulation. Also, the relative merits of a single asymmetric strake versus double strakes were investigated. The flow-field studies suggested plausible flow mechanisms to explain the aerodynamic asymmetries produced by different strake arrangements. The force and moment results showed that a single strake, located between 105^{o} and 120^{o} from the windward meridian had considerable yaw control potential in the alpha range from 20^{o} to 80^{o} (the test limit). The low Reynolds number results of this investigation, although providing a valid preliminary assessment of the basic concept, require verification with respect to scale effects.

Acknowledgment

This research is jointly supported by NASA Langley Research Center and U.S. Air Force Wright Aeronautical Laboratory. The encouragement and support received from Joseph L. Johnson (NASA Langley) and Dieter Multhopp (AFWAL) are greatly appreciated.

References

1. Hunt, B. L.: Asymmetric Vortex Forces and Wakes on Slender Bodies. AIAA Paper No. 82-1336, September 1982.

2. Skow, A. M., Moore, W. A. and Lorincz, D. J.: Forebody Vortex Blowing - A Novel Control Concept to Enhance Departure/Spinning Recovery Characteristics of Fighter and Trainer Aircraft. AGARD CP No. 262, Paper No. 24, 1979.

3. Carr, P. C. and Gilbert, W. P.: Effects of Fuselage Forebody Geometry on Low-Speed Lateral-Directional Characteristics of Twin-Tail Fighter Model at High Angles of Attack. NASA TP 1592, December 1979.

4. Rao, D. M. and Murri, D. G.: Exploratory Investigation of Deflectable Forebody Strakes for High-Angle-of-Attack Yaw Control. AIAA Paper No. 86-0333, January 1986.

5. Lockwood, V. E. and McKinney, L. W.: Effect of Reynolds Number on the Force and Pressure Distribution Characteristics of a Two-Dimensional Lifting Circular Cylinder. NASA TN D-455, September 1960.

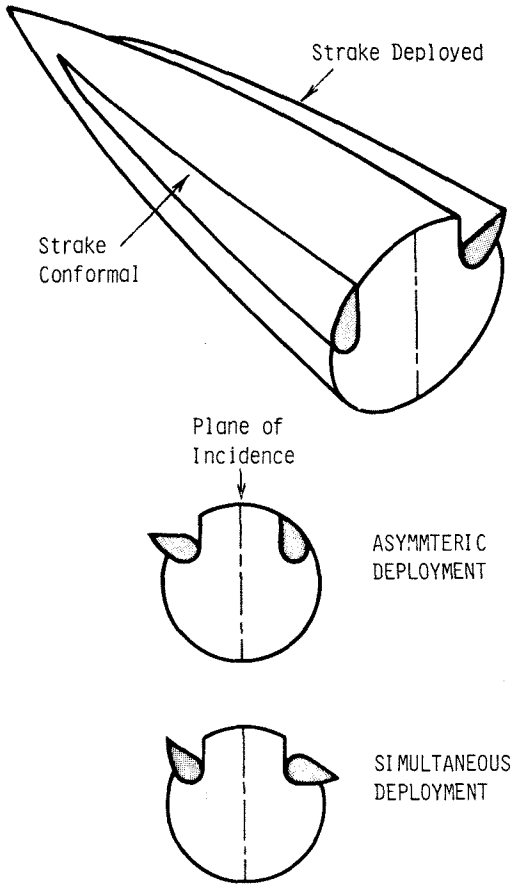

Fig. 1. Deployable Forebody Strake Concept

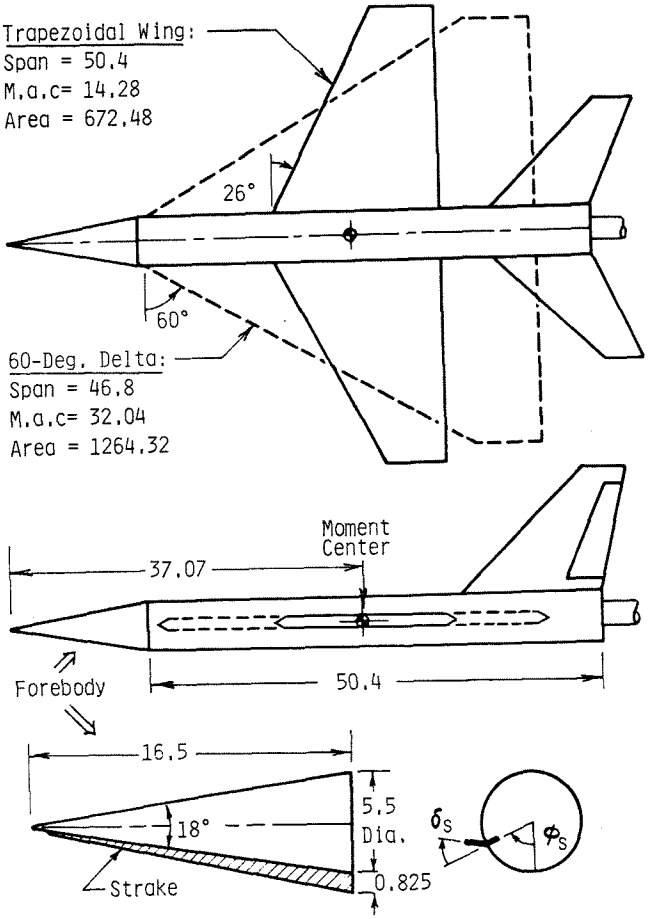

Fig. 2. Wind Tunnel Model of Generic Fighter Configurations (Dimensions in inches)

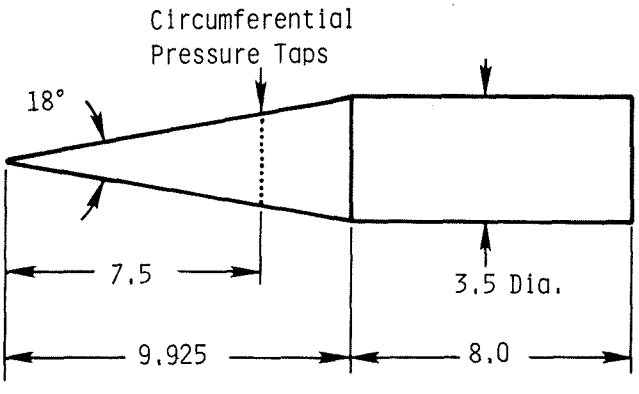

Fig. 3. Isolated Forebody Model for Flow Visualization and Pressure Surveys (Dimensions in inches)

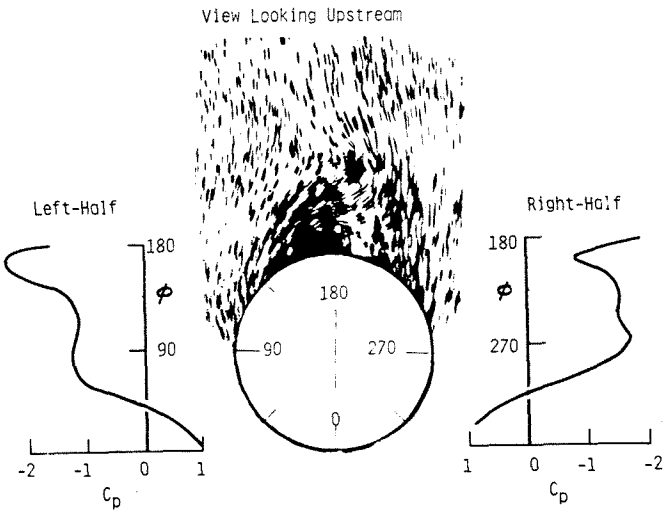

Fig. 4. Flow Visualization and Pressure Distribution on Basic Forebody (strake off) at $\alpha = 50^{\circ}$

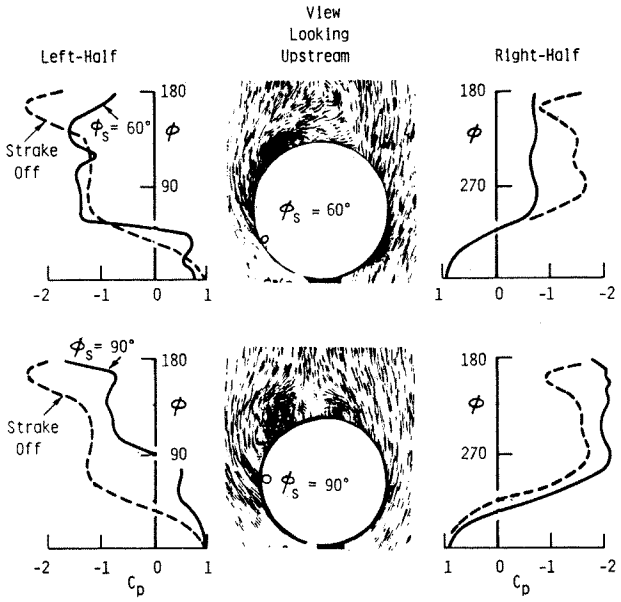

Fig. 5. Flow Visualization and Pressure Distribution with Single Strake at ϕ_s = 60 and 90°

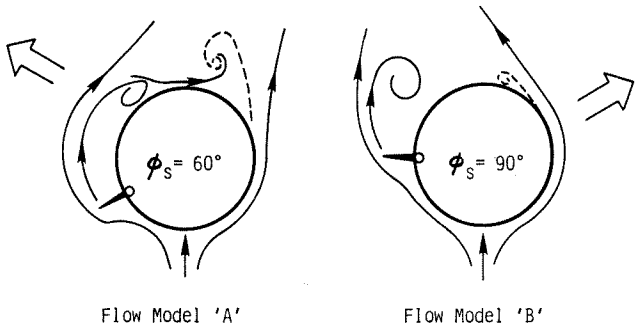

Fig. 6. Suggested Cross-Flow Models Generating Opposite Side Forces with ϕ_s = 60 and 90°

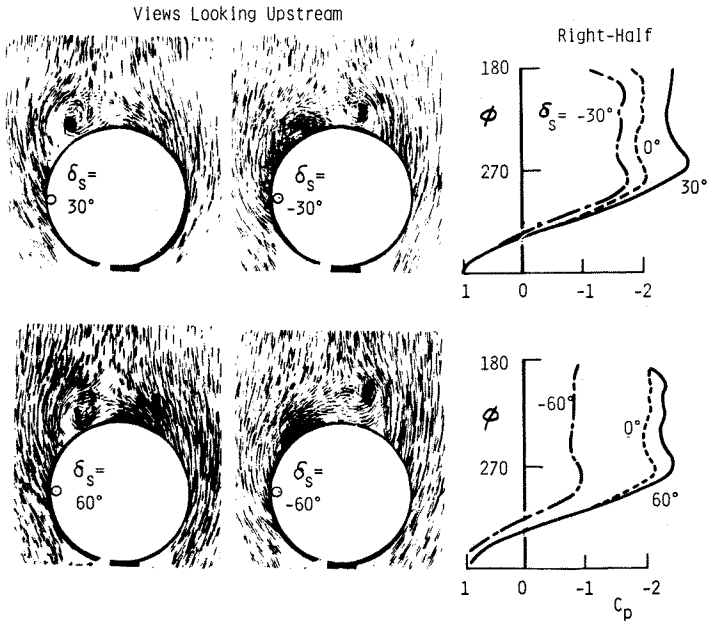

Fig. 7. Flow Visualization and Right-Half Pressure Distributions with Single Strake at ϕ_s = 90° Showing Effect of Strake Deflection

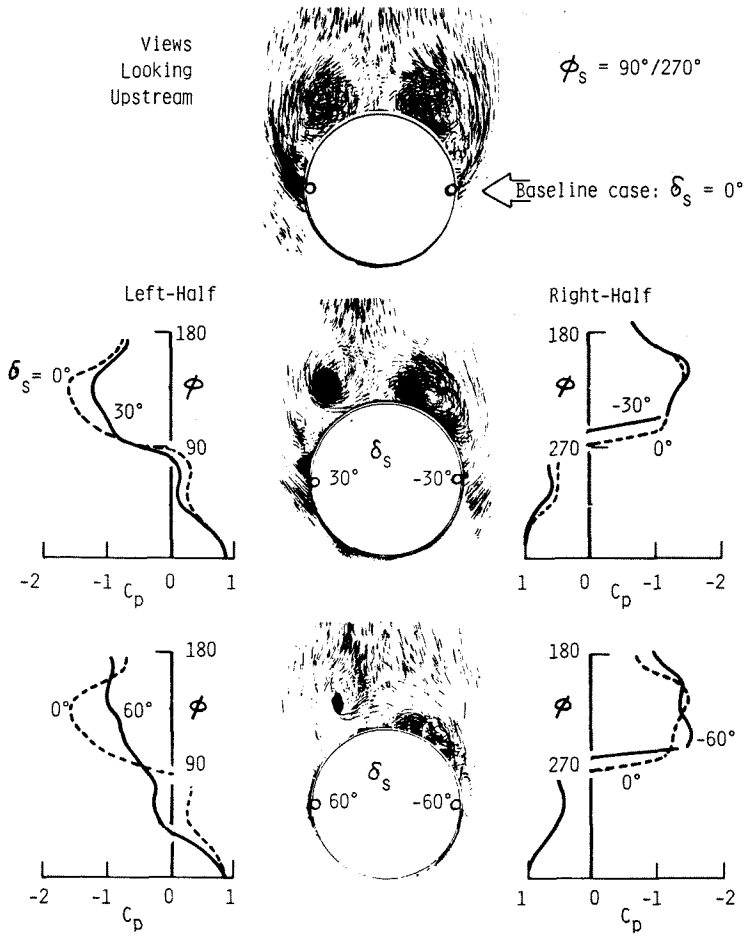

Fig. 8. Flow Visualizations and Pressure Distributions with Double Strakes at ϕ_s = 90/270° Showing Effect of Anit-Symmetric Deflection

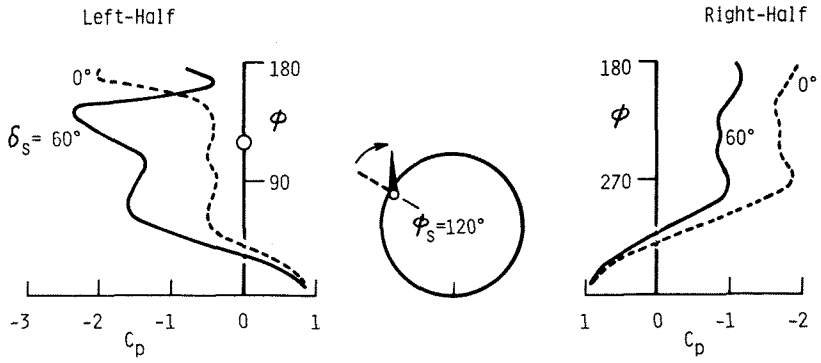

Fig. 9. Pressure Distributions with Single Strake at ϕ_s = 120° Showing Effect of Deflection

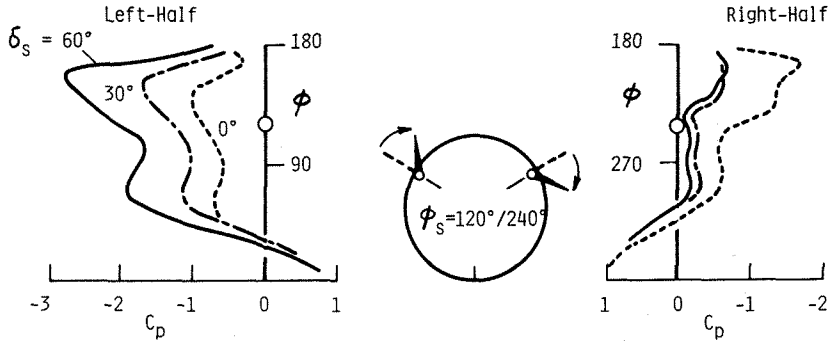

Fig. 10. Pressure Distributions with Double Strakes ϕ_s = 120/240° Showing Effect of Anti-Symmetric Deflection

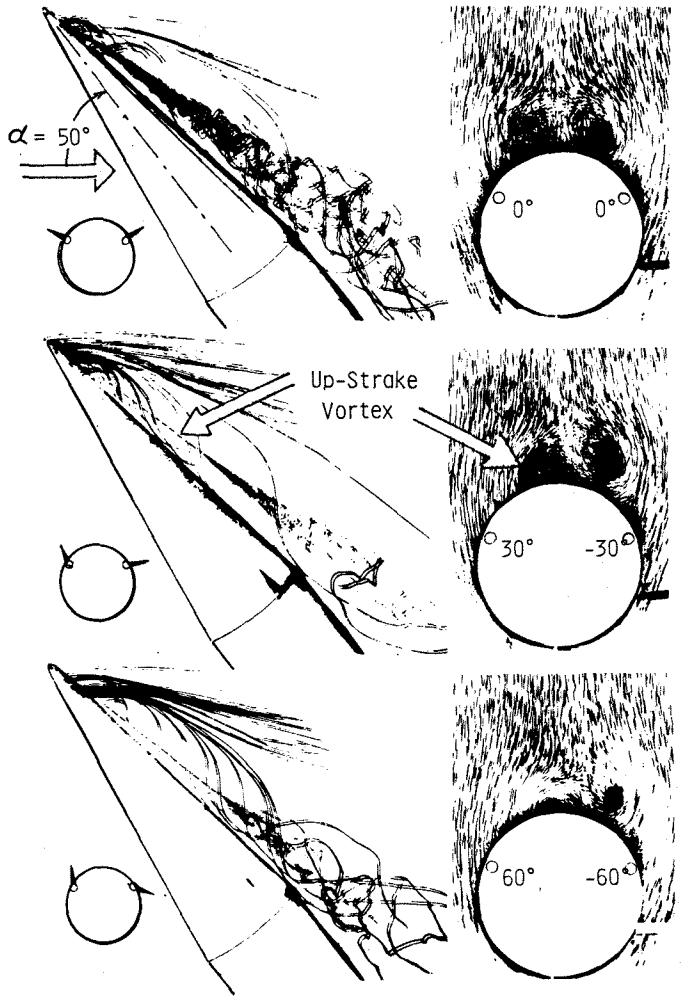

Fig. 11. Side-View and Cross-Flow Visualizations with Double Strakes at ϕ_s = 120/240° Showing Effect of Anti-Symmetric Deflection

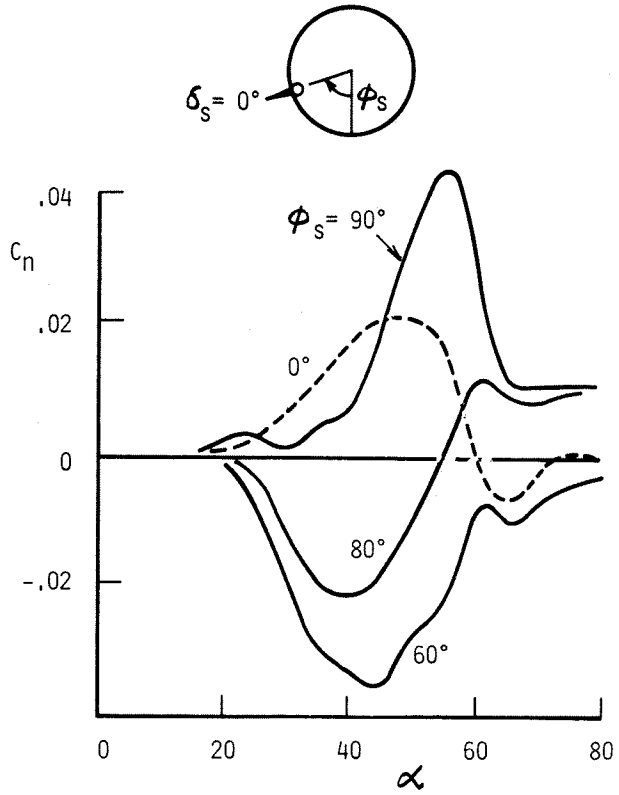

Fig. 12. Yawing Moment Characteristics of Fuselage with Single Strake at ϕ_s = 60 to 90°

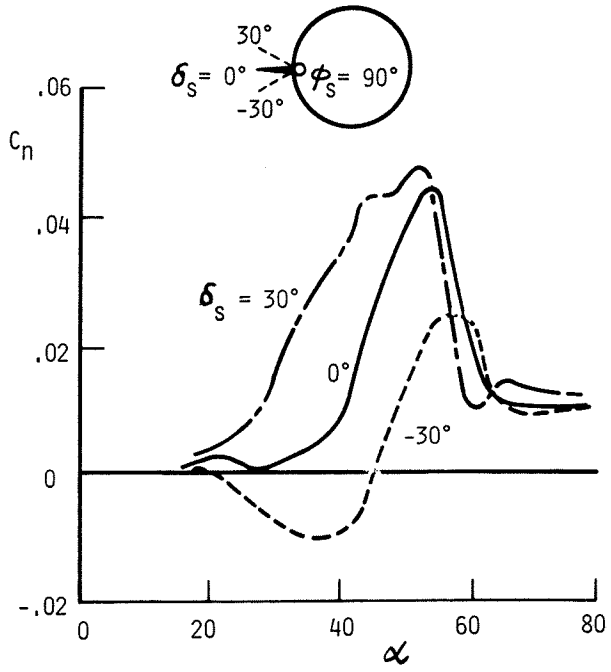

Fig. 13. Yawing Moment Characteristics of Fuselage with Single Strake at ϕ_s = 90° Showing Effect of Deflection

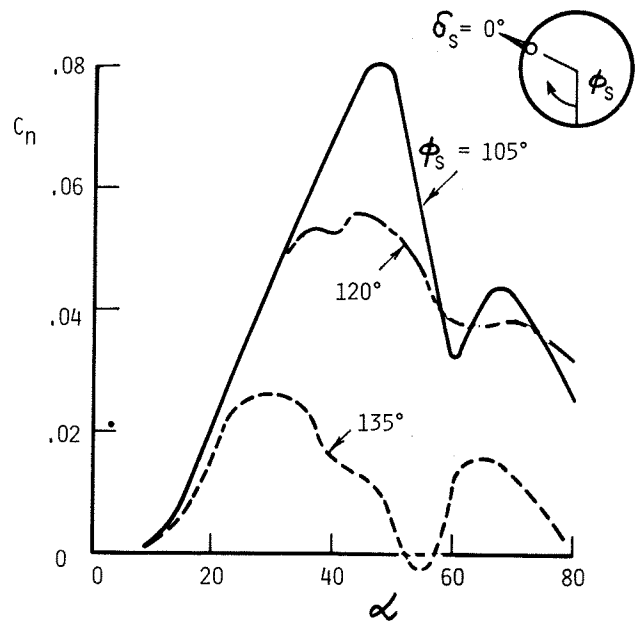

Fig. 14. Yawing Moment Characteristics of Fuselage with Single Strake at ϕ_s = 120 to 135°

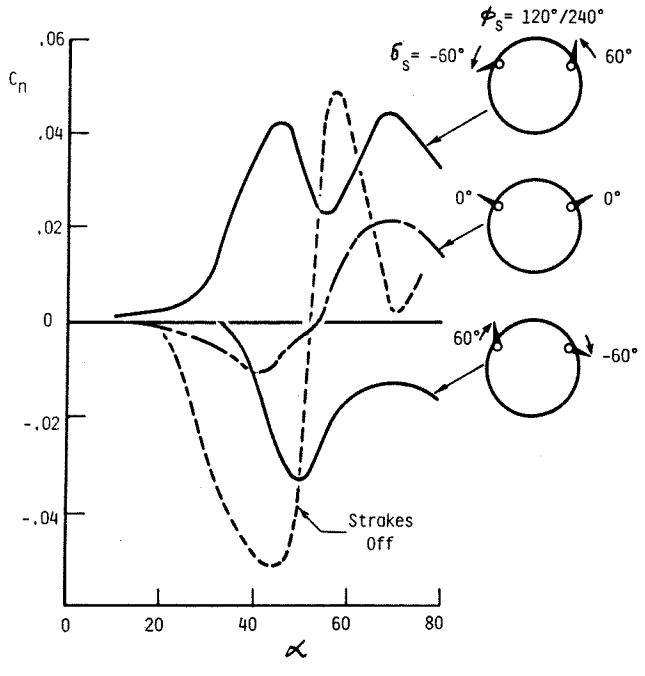

Fig. 15. Yawing Moment Characteristics of Fuselage with Double Strakes at ϕ_s = 120/240°

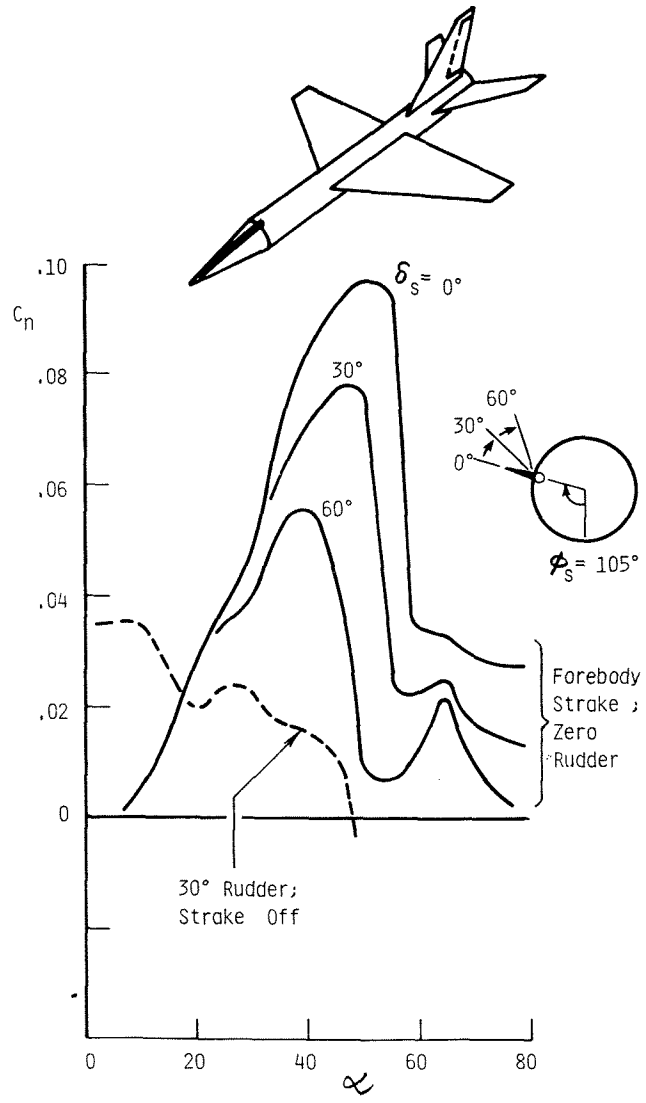

Fig. 16. Yawing Moment Characteristics of Trapezoidal-Wing Configuration with Single Strake at $\phi_s = 105^o$ in Comparison with Rudder

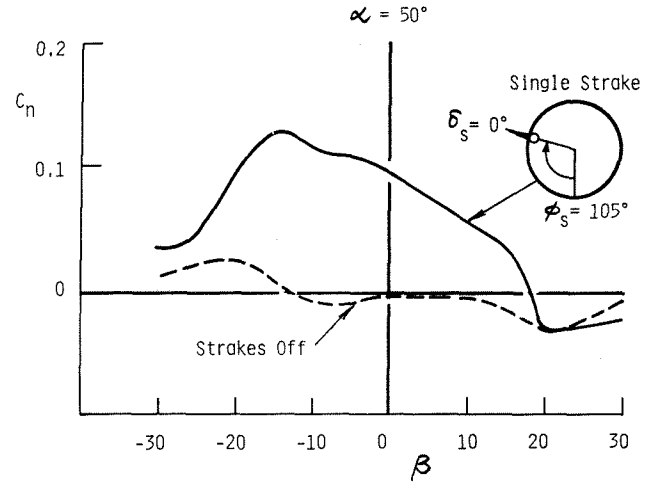

Fig. 17. Yawing Moment Characteristics with Side-Slip of Trapezoidal-Wing Configuration with Single Strake at $\phi_s = 105^o$

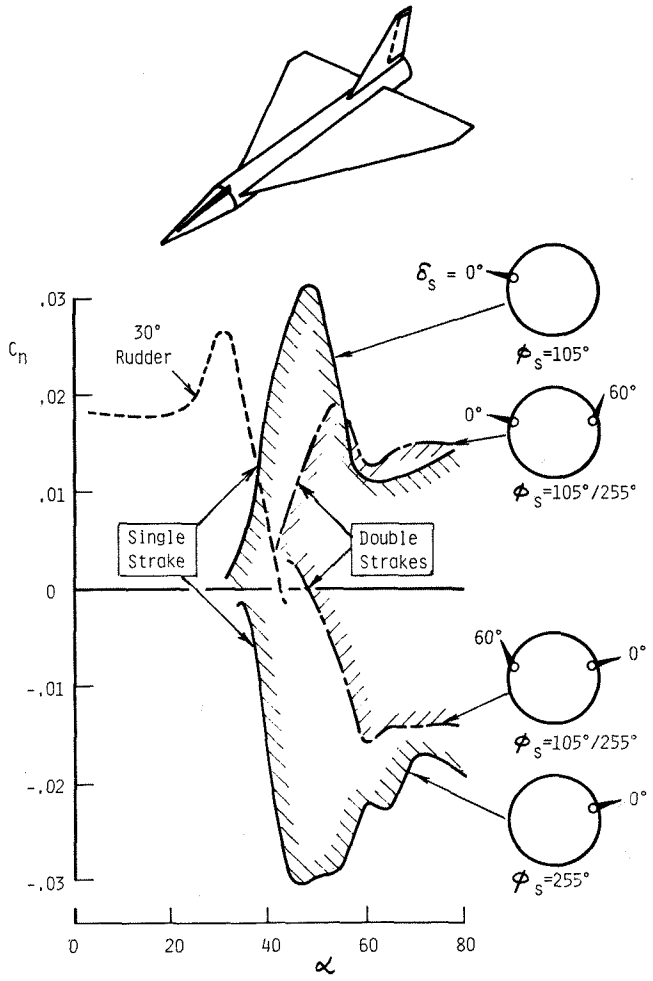

Fig. 18. Yawing Moment Characteristics of Delta-Wing Configuration with Single and Double Strakes in Comparison with Rudder

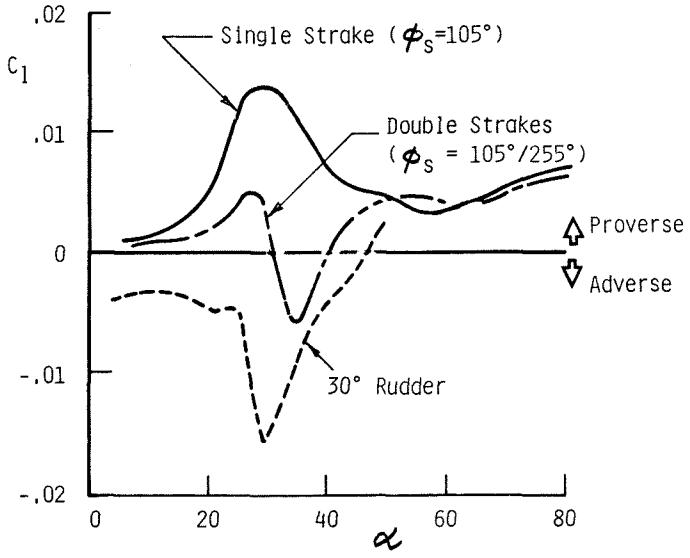

Fig. 19. Induced Roll Characteristics of Delta-Wing Configuration with Strakes in Comparison with Rudder.

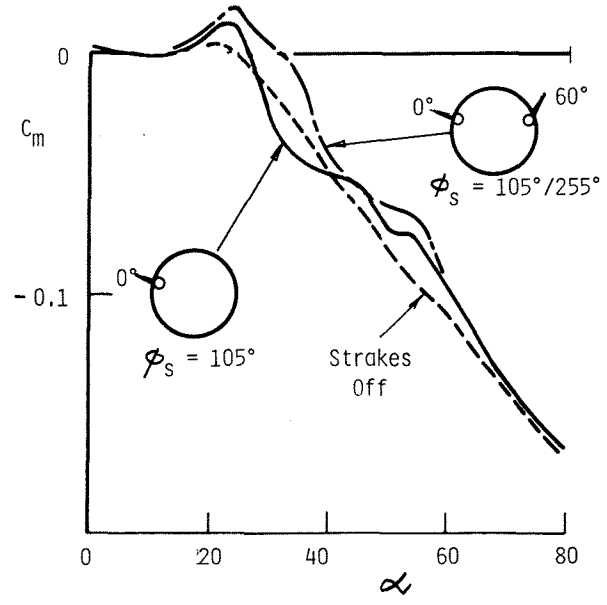

Fig. 20. Pitching Moment Characteristics of Delta-Wing Configuration with Strake Deployment